JOURNAL OF MULTIDISCIPLINARY ADAPTIVE CLIMATE INSIGHTS
(MACI) Volume 3, Issue 1, June 2026 - E-ISSN 3009-6332

http://dx.doi.org/10.21622/MACI.2026.03.1.1985

Assessing RegCM4 Simulations of the Diurnal Temperature Range over Egypt: Sensitivity to Soil Moisture Initialization and Land-Surface Parameterization

Samy A. Anwar *

Egyptian Meteorological Authority, Qobry EL-Kobba, Cairo, Egypt.

ratebsamy@yahoo.com

Received: 09 March 2026 Accepted: 05 April 2026 Published: 19 May 2026

Abstract:

This study investigates the impact of soil moisture initialization and land-surface parameterization on Egypt's diurnal temperature range (DTR) using the regional climate model RegCM4. Four 40-year simulations were conducted for the period 1979–2018, representing different combinations of soil moisture datasets and hydrological schemes. Soil moisture was initialized using two products: the ESA Climate Change Initiative (ESA) satellite dataset and the Century (CEN) reanalysis dataset. In addition, two hydrological schemes were applied: TOPMODEL (TOP) and the Variable Infiltration Capacity model (VIC). All simulations were evaluated against the high-resolution TerraClimate dataset and in situ station observations.

The results indicate that daily maximum temperature (TMX) is largely insensitive to both soil moisture initialization and parameterization schemes, whereas daily minimum temperature (TMN) and DTR exhibit strong sensitivity. Simulations initialized with the ESA dataset generally produce warmer TMN values than those initialized with the CEN dataset, with biases ranging from 2–4°C along the Mediterranean coast and 2–6°C across much of Egypt. A similar sensitivity is observed between the TOP and VIC hydrological schemes. Overall, the CEN–TOP configuration provides the most accurate simulation of DTR across all seasons.

Comparison with station observations reveals that DTR biases vary by location, with both overestimation and underestimation depending on the station. Application of a linear scaling (LS) bias-correction method significantly reduces these biases. These findings suggest that accurate simulation of Egypt's DTR can be achieved when RegCM4 is initialized with the CEN soil moisture dataset, coupled with the TOP hydrological scheme, and corrected using LS.

Keywords: DTR, Soil moisture initialization, Soil moisture parameterization, RegCM4, Linear-scaling.

* Corresponding author

1. Introduction

Climate change significantly affects atmospheric variables such as temperature and precipitation, including their extremes (IPCC, 2021). Daily maximum and minimum air temperatures are key indicators of climate variability and change, reflecting both natural variability and anthropogenic influences (Ritchie and Roser, 2019). The diurnal temperature range (DTR), defined as the difference between daily maximum and minimum temperatures, is a widely used metric for detecting climate change signals due to its sensitivity to variations in the surface energy balance (Braganza et al., 2004; Ongoma et al., 2020). In meteorological terms, hot days are typically defined as days when temperatures exceed a specified high-percentile threshold (e.g., the 90th or 95th percentile), while heat wave (HW) days refer to periods of consecutive hot days (usually lasting at least 3–5 days). In contrast, typical summer days represent climatological average conditions without extreme temperature anomalies.

DTR plays an important role across multiple sectors, including human health, agriculture, ecosystems, and energy demand (Davis et al., 2020; Huang et al., 2020; Adekanmbi et al., 2022; Bravo et al., 2020). Its variability is controlled by several factors, including cloud cover, land use, aerosols, and land–atmosphere interactions, particularly soil moisture (Dai et al., 1999; Ren et al., 2014; Schultz et al., 2017). Observational studies have shown that increased cloudiness and soil moisture tend to reduce DTR by suppressing daytime heating and enhancing nighttime temperatures (Stone and Weaver, 2003; Wang et al., 2014). In contrast, drier conditions enhance sensible heating and increase DTR through reduced evapotranspiration (Panwar et al., 2020).

Modeling studies further highlight the complex role of land–atmosphere processes in shaping DTR variability. For example, vegetation dynamics, aerosols, and radiative forcing have been shown to modulate DTR differently across regions and climate regimes (Jeong et al., 2011; Katavoutas et al., 2023; Roesch et al., 2025). Despite these advances, uncertainties remain regarding the representation of soil moisture processes in regional climate models and their impact on temperature extremes.

In the context of Egypt, previous modeling studies using RegCM4 have demonstrated that soil moisture initialization significantly affects simulated temperature fields. For instance, initializing the model with soil moisture data improves the representation of soil and near-surface air temperatures compared to bare soil conditions (Anwar, 2023; Anwar and Mostafa, 2023). However, the combined effects of soil moisture initialization and parameterization on DTR have not been comprehensively investigated. This study aims to quantify the impact of soil moisture initialization and parameterization on the DTR over Egypt using RegCM4. Specifically, it evaluates how these factors influence daily TMX and TMN, and examines the effectiveness of linear scaling (LS) bias correction in improving the representation of the DTR annual cycle. This work represents the first systematic assessment of soil moisture–DTR interactions in Egypt using RegCM4, providing a reference for future regional modeling studies and climate adaptation planning.

2. Materials and Methods

2.1. Study area

Egypt is located in the North Africa and Middle East (MENA) region, bordered by the Mediterranean Sea to the north, the Red Sea to the east, and Libya to the west, and the Sinai Peninsula to the northeast, extending between latitudes 22°N–32°N and longitudes 24°E–37°E. The country covers approximately 1,000,000 km² and exhibits diverse topography, ranging from the Western Desert, lying around 133 m below mean sea level, to elevated terrain in the Sinai Peninsula, including Mount Catherine at 2,642 m above sea level. The Nile Valley and Delta are the primary population centers.

Climatically, Egypt is classified as a hot desert (BWh) according to the Köppen system (El-Kenawy et al., 2010; Hamed et al., 2022a, b), with pronounced spatial and temporal variability. Based on annual rainfall, six climatic regions are commonly recognized:

1. **Mediterranean Coast:** ~200 mm/year, mainly from cyclonic activity.
2. **Nile Delta:** ~25 mm/year, largely dependent on irrigation.
3. **Central Egypt:** ~10 mm/year.
4. **Upper Egypt:** minimal rainfall, dependent on Nile water.

http://dx.doi.org/10.21622/MACI.2026.03.1.1985

5. **Red Sea Coast:** infrequent but intense rainfall events cause flash floods.

6. **Sinai Mountains:** >100 mm/year due to orographic effects, supporting small-scale agriculture.

Egypt experiences two main seasons: a hot, dry period from May to October, and a cooler season from November to April, when precipitation can reach up to 200 mm in northern regions but drops below 20 mm in southern areas. Regionally, annual air temperature variability can be summarized as:

1. **Mediterranean Coast:** winter 13–21 °C, summer 24–32 °C.

2. **Nile Valley and Delta:** winter 14–20 °C, summer up to 40 °C.

3. **Western and Eastern Deserts:** winter 8–18 °C, summer >45 °C.

4. **Southern Egypt:** summer >40 °C, mild winters with cold nights (Hamed et al., 2022a).

The arid climate, combined with this spatial heterogeneity, makes Egypt highly sensitive to climate change impacts, including increased frequency and intensity of heatwaves, extended drought periods, and water scarcity, with significant implications for agriculture and public health (Nashwan et al., 2020).

2.2. RegCM model description and experiment design

This study investigates the sensitivity of Egypt's DTR to soil moisture initialization and land-surface parameterization using the Regional Climate Model version 4 (RegCM4; Giorgi et al., 2012). Simulations were dynamically downscaled using the ERA-Interim reanalysis (EIN15; Dee et al., 2011) at a horizontal resolution of 25 km, which provides the initial and lateral boundary conditions. Although higher-resolution products such as ERA5 are available, ERA-Interim was selected due to its extensive validation in regional climate modeling studies, including RegCM4 applications over North Africa, ensuring consistency with previous work. In addition, the multi-decadal simulations and multiple sensitivity experiments conducted in this study impose considerable computational and data storage demands, for which ERA-Interim provides a practical balance between resolution and efficiency. Furthermore, ERA-Interim offers sufficiently reliable large-scale atmospheric forcing for assessing the relative sensitivity of DTR to soil moisture initialization and parameterization.

The Egyptian domain spans 24–38°E and 22–34°N, with 60 grid points applied in both zonal and meridional directions to minimize lateral boundary buffer effects (Figure 1; Anwar and Olusegun, 2024). The model is configured in hydrostatic mode (Grell et al., 1994a,b) with 18 terrain-following sigma levels, the Emanuel cumulus scheme (Emanuel and Zivkovic-Rothman, 1999) using a tuned precipitation efficiency parameter (omtrain = 0.777), the UW planetary boundary layer scheme (Grenier and Bretherton, 2001), and the RRTM radiation scheme (Kiehl et al., 1996). The simulation period extends from 1979 to 2018, with the first two years treated as spin-up to stabilize soil moisture and energy fluxes (Steiner et al., 2009), while analyses focus on 1981–2018.

Soil moisture was initialized using two independent datasets: the ESA Climate Change Initiative (ESACCI; Dorigo et al., 2017; Gruber et al., 2019) satellite product (0.25° resolution) and the Century (CEN) global reanalysis dataset from NOAA (Slivinski et al., 2019; 1° resolution). To evaluate soil hydrology effects, two CLM45 (Community Land Model v4.5; Oleson et al., 2013) schemes were applied: TOPMODEL (TOP; Niu et al., 2005) and the Variable Infiltration Capacity model (VIC; Liang et al., 1994, 1996a, b, 2003). These schemes differ in their representation of soil moisture dynamics and runoff generation, allowing a clear separation of soil moisture initialization versus parameterization effects on DTR. The four 40-year experiments are grouped as follows: (i) soil moisture parameterization experiments using CEN initialization with TOP and VIC schemes, and (ii) soil moisture initialization experiments using the TOP scheme with ESA and CEN datasets.

The CLM45 model simulates key biogeophysical and hydrological processes governing land–atmosphere interactions, including radiation fluxes, sensible and latent heat fluxes, soil heat transfer, and runoff generation. Key soil hydrology parameters follow the standard CLM45 implementation and were tuned to ensure physically consistent differences between TOP and VIC schemes. Sensitivity experiments showed that omtrain = 0.777 produces a meaningful distinction between the two schemes, whereas omtrain = 0.999 suppresses these differences (Anwar et al., 2019).

Surface and atmospheric variables analyzed include soil moisture (SM, in mm), radiation fluxes (RSDS, RSNS, RLDS, RLNS, in W m^{-2}), ground temperature (TS, in °C), sensible heat flux (SHF, in W m^{-2}), and near-surface relative humidity (RH, in %). RSDS and RSNS stand for the global and net incident solar radiation, while RLDS and RLNS stand for the global and net incident longwave radiation.

Daily maximum (TMX, in °C) and minimum (TMN, in °C) air temperatures were used to compute DTR (DTR = TMX - TMN, in °C). While other meteorological factors (e.g., cloud cover, wind speed, and atmospheric moisture) also influence DTR, this study focuses on soil moisture–driven changes, which are implicitly represented within the RegCM4 physics and associated fluxes.

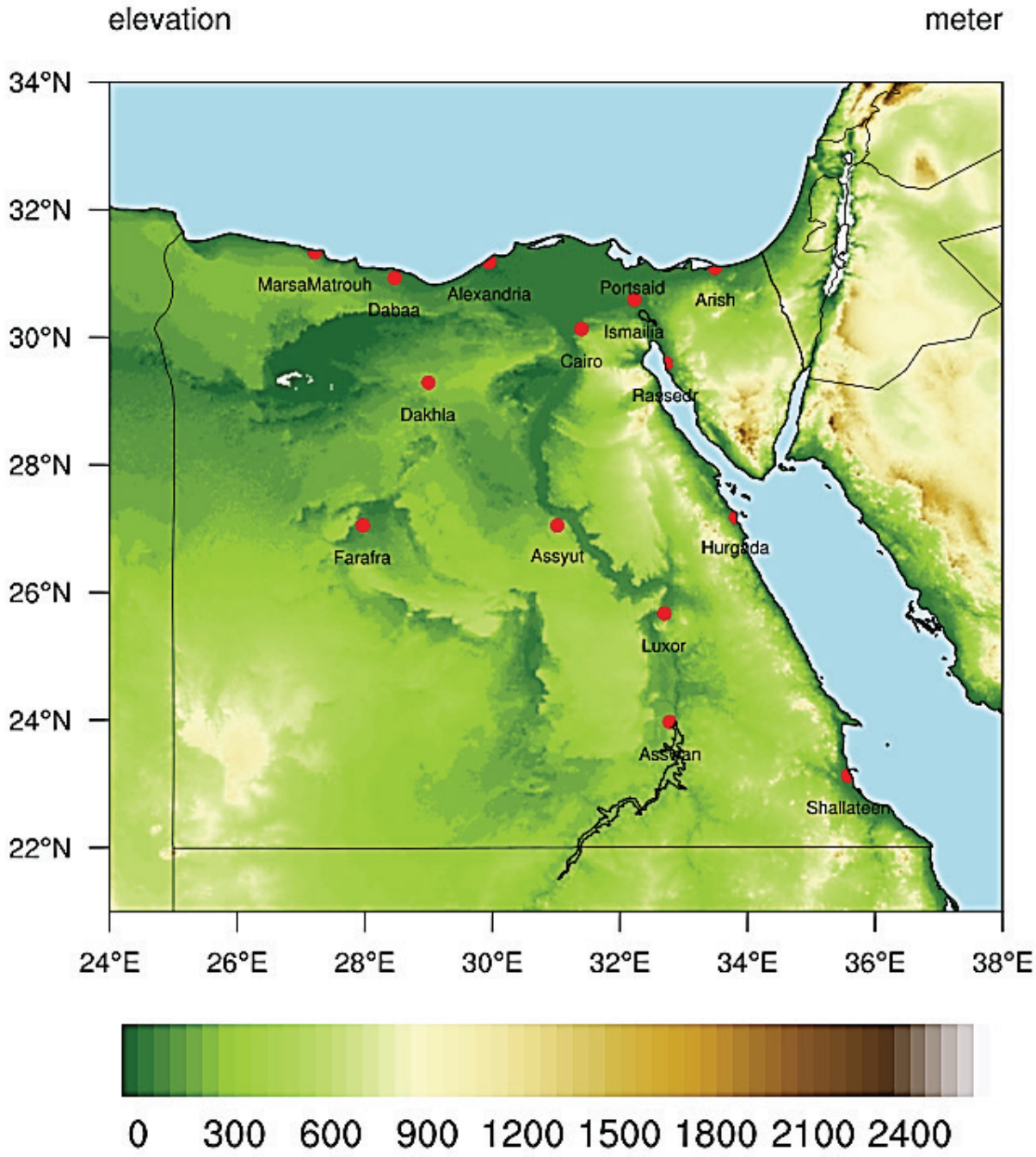

Figure 1: Topography of Egypt (elevation above mean sea level) and locations of the 15 meteorological stations used for evaluating RegCM4 simulations of diurnal temperature range (DTR). Station records span 1981–2018 and represent diverse climatic and geographic regions. Red dots indicate station locations; note that Ismailia does not have complete data, which is why only 14 dots appear on the map.

http://dx.doi.org/10.21622/MACI.2026.03.1.1985

Table 1: RegCM4 configuration and experimental design adopted to assess the effects of soil moisture initialization and parameterization

Model domain	24 to 38°E and from 22 – 34°N, res. = 25 km; clat = 27, clon = 30 and iy = jx = 60
Map projection	Rotated Mercator
Vertical coordinate	Terrain-following sigma coordinate; Total: 18 sigma levels
Cumulus parameterization	Emanuel scheme (with precipitation efficiency; omtrain = 0.777) over land and Ocean
Land surface model	Community Land Model version 4.5 (CLM45)
Radiation parameterization	RRTM radiation scheme (with default parameters)
PBL parameterization	UW boundary layer scheme (with default parameters)
Lateral boundary condition	ERA-Interim Reanalysis 1.5° x 1.5°
Sea surface temperature (SST) boundary condition	ERA-Interim Reanalysis 1.5° x 1.5°
Soil moisture initialization	ESACCI satellite product (ESA) and Century reanalysis (CEN)
Soil moisture parameterization	TOP and VIC soil moisture schemes of the CLM45 land surface model

2.3. Observational dataset

To evaluate the simulated DTR, two observational datasets were used. First, the high-resolution TerraClimate dataset (TERRA) was employed to evaluate DTR at each grid point, as it integrates multiple reanalysis and observational products. TERRA combines climatological information from WorldClim with temporally varying data from coarser-resolution products, including the Climate Research Unit Time Series version 4.0 (CRU TS4.0; Harris et al., 2020) and the Japanese 55-year Reanalysis (JRA-55; Kobayashi et al., 2016). By interpolating CRU anomalies onto the WorldClim climatology, TERRA provides long-term, high-resolution (~4 km) data, including temperature-based metrics and derived hydro-climatic variables such as reference evapotranspiration (ET_o), soil moisture, runoff, and the Palmer Drought Severity Index. For the evaluation of RegCM4 outputs, TERRA was bilinearly interpolated onto the model's curvilinear grid, and the statistical significance of biases was examined using a Student's t-test at $\alpha = 0.05$.

Second, observational data on daily TMX and TMN were collected from 15 meteorological stations distributed across Egypt, representing diverse climatic and geographic regions (Figure 1; Table 2). Station records span 1981–2018, consistent with the RegCM4 simulations. All data underwent rigorous quality control, including checks for missing values, outliers, and inconsistencies, and were cross-validated with neighboring stations and the TERRA dataset to ensure reliability. These high-quality station observations provide a robust benchmark for evaluating model performance at the local scale.

Table 2: The table shows station coordinates, World Meteorological Organization (WMO) ID, and elevation above mean sea level (in meters)

Station	WMO Code	Longitude (°E)	Latitude (°N)	Elevation (m)
Marsa-Matrouh	62306	27.22	31.33	25
Dabaa	62309	28.47	30.93	17
Alexandria	62318	29.95	31.18	-2.626
Port Said	62332	32.20	31.28	0.8
Arish	62337	33.49	31.09	30.57
Cairo	62366	31.40	30.13	64.12
Assyut	62393	31.02	27.05	226
Luxor	62405	32.70	25.67	83.64
Asswan	62414	32.78	23.97	192.53
Farafra	62423	27.97	27.05	77.79
Dakhla	62432	29.00	25.29	107.26
Ismailia	62440	32.23	30.59	10.14
Ras Sedr	62455	32.72	29.59	3.26
Hurgada	62463	33.82	27.18	7.79
Shallateen	62476	35.58	23.13	19.44

The DTR was calculated by taking TMX and subtracting TMN from it. The ideal configuration (of the initialized/parameterized soil moisture) will be evaluated against the OBS climatological annual pattern. Ultimately, the improved value of the linear scaling (LS) bias-correction method is attained by

integrating the seasonal mean into every season of the simulation as follows:

$$RCMnew_i = RCM_i + (OBS_{seasonal} - RCM_{seasonal}) \quad (1),$$

where i represents the season (winter, spring, summer, and autumn), RCM_i denotes the uncorrected output from RegCM4, and $RCMnew_i$ indicates the bias-adjusted output from RegCM4. $OBS_{seasonal}$ represents the seasonal mean of the OBS, while $RCM_{seasonal}$ denotes the seasonal mean of the RegCM4. To analyze the additional benefit of the LS, the Taylor diagram (Taylor 2001) was utilized. Essentially, the Taylor diagram requires three statistical measures: Standard deviation ratio (STD), Mean bias (MB), and Spatial correlation coefficient (CORR). The Taylor diagram provides a quantitative summary for comparing two or more model configurations across multiple locations within a single figure. It allows assessment of model performance by displaying key statistical metrics, including the correlation coefficient (CORR, ranging from -1 to 1, where -1 indicates a perfect negative correlation and 1 indicates a perfect positive correlation), mean bias (MB, expressed in absolute terms or as a percentage), and standard deviation (STD, ranging from 0 to 1.65), which reflects the consistency of model variance relative to observations.

3. Results and Discussion

The influence of soil moisture initialization and parameterization on maximum temperature (TMX), minimum temperature (TMN), and DTR was assessed using a diagnostic analysis (Figures 2 and S1–S5). Soil moisture at 10 cm depth was examined first, followed by related radiative and thermal variables to understand their effects on temperature responses. Seasonal climatologies of TMX and TMN were analyzed for each experiment to identify which temperature component is most sensitive to soil moisture configuration and to determine the setup that minimizes DTR bias relative to the TERRA dataset. The analysis was performed for the four climatological seasons: spring (MAM), summer (JJA), autumn (SON), and winter (DJF).

The observed sensitivity of DTR to soil moisture initialization and parameterization aligns with general physical principles documented in global studies. Drier soils in the CEN-TOP configuration enhanced daytime sensible heating, resulting in increased DTR, while wetter conditions promoted latent heat flux, which cooled the surface and reduced nighttime warming, consistent with findings by Dai et al. (1999) and Panwar et al. (2020). Although these mechanisms have not been directly investigated in Egypt, they provide a robust framework for interpreting our results.

3.1. Influence on the TMX/TMN

Figure 2 presents the simulated soil moisture (SM) for the TOP and VIC experiments (Figures 2a and 2b) along with the significant differences between VIC and TOP (Figure 2c). Statistical significance at each grid point was assessed using a Student's t-test with $\alpha = 0.05$. Overall, VIC (Figure 2b) produces higher soil moisture than TOP (Figure 2a) across Egypt. Quantitatively, this difference ranges from 7.5 to 17.5 mm, reaching nearly 30 mm in the Nile Delta region (26–34°E, 28–34°N; Figure 2c). A similar pattern is observed when comparing the ESA and CEN initializations: ESA (Figure 2e) exhibits greater soil moisture than CEN (Figure 2d), with the ESA–TOP difference closely resembling the VIC–TOP difference (Figure 2f). Analysis of radiative fluxes indicates that soil moisture initialization has little effect on incoming shortwave radiation (RSDS, W m²; Figures S1 a–c), net surface solar radiation (RSNS, W m^{-2}; Figures S1 d–f), or incoming longwave radiation (RLDS, W m^{-2}; Figures S1g–i). However, differences are evident in net downward longwave radiation (RLNS, W m^{-2}), with VIC exhibiting 6–10 W m^{-2} higher RLNS than TOP (Figure S1 l). As a result, surface temperature (TS, °C) is 1–3°C warmer under VIC compared to TOP (Figure S2 c). In neither contrast, neither sensible heat flux (SHF, W m^{-2}) nor 2 m relative humidity (RH, %) show significant differences between the TOP and VIC simulations (Figures S2 f, i).

Figure S3 demonstrates that RegCM4 accurately reproduces the spatial patterns of maximum temperature (TMX, °C) relative to TERRA across all seasons (Figures S3 a–c, g–i, m–o, and s–u). Both TOP and VIC simulations exhibit a persistent cold bias in TMX across seasons, which is particularly pronounced during summer (JJA) and winter (DJF) (Figures S2j, k, and v, w). Notably, no significant differences are observed between the two simulations in any season. This behavior can be attributed to the minimal influence of the TOP/VIC soil moisture schemes on net surface solar radiation (RSNS) and sensible heat flux (SHF), which limits their effect on TMX despite differences in surface temperature (TS). Seasonally, the cold bias in spring

http://dx.doi.org/10.21622/MACI.2026.03.1.1985

(MAM) ranges between 1 and 4°C (Figures S3 d, e). In summer (JJA), a warm bias of 1–4°C occurs along the Mediterranean and Red Sea coasts, whereas a cold bias of 2–6°C dominates much of Egypt, particularly within 24–28°E and 22–26°N. During winter (DJF), a widespread cold bias of 1–5°C is observed throughout the country (Figures S3 v, w).

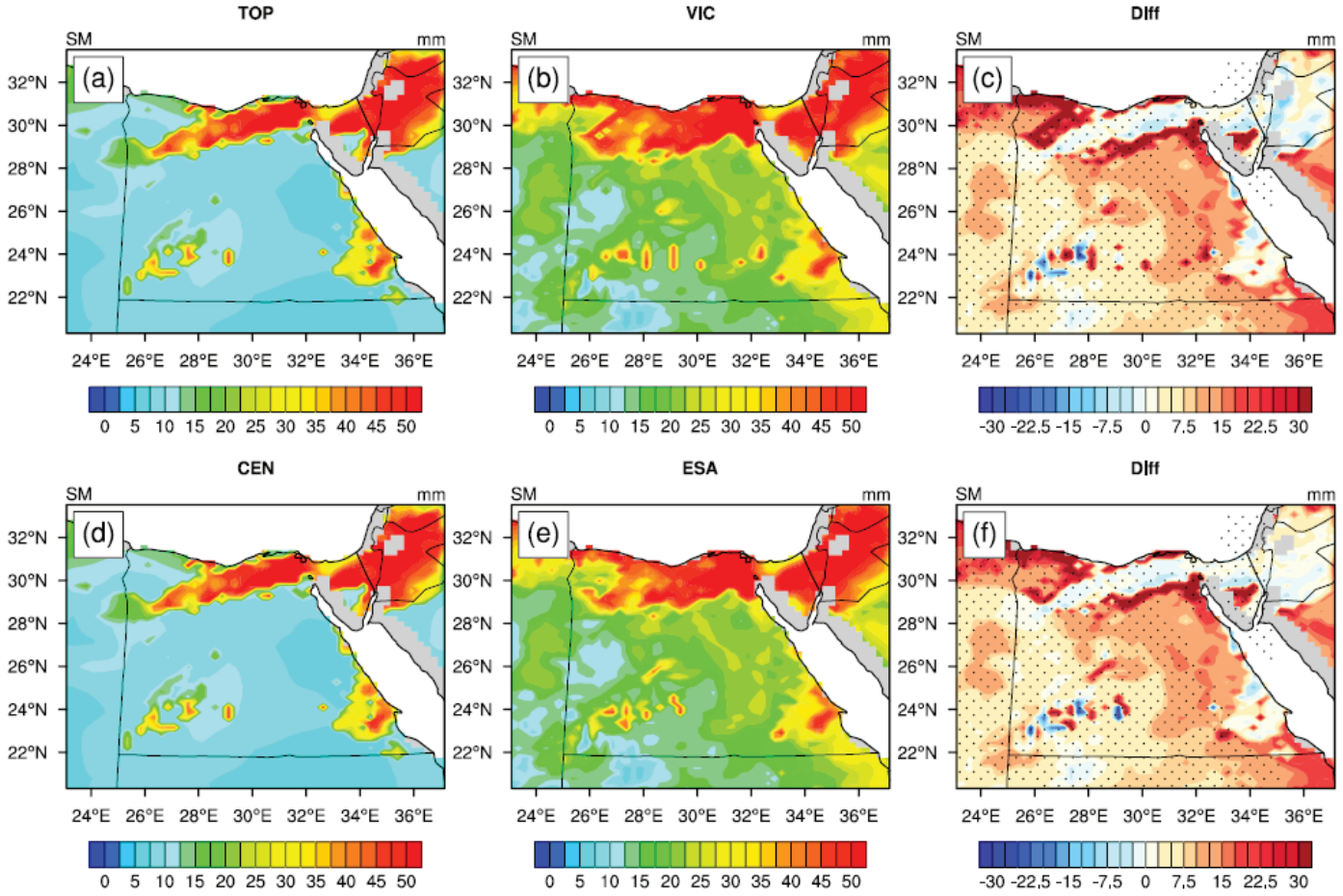

Figure 2: Soil moisture of depth 10 cm (SM; mm).
The first row (a-c) shows the two simulations: TOP and VIC, and their significant difference.
The second row shows the two simulations: ESA and CEN, and their significant difference during the period 1981 - 2018.
Note that the significant difference was calculated using a Student's t-test with α=0.05

In contrast to TMX, notable differences between the TOP and VIC simulations are evident for minimum temperature (TMN, °C; Figure 3). For example, during the MAM season, the TOP simulation exhibits a warm bias of 1–3.5°C, primarily in the region between 28–32°E and 28–30°N, while other areas show a cold bias of 1–1.5°C, reaching up to 2°C in some locations (Figure 3d). In comparison, VIC generally produces a warm bias across Egypt, ranging from 1 to 5.5°C, with localized values reaching up to 6°C (Figure 3e). Overall, VIC is 2–5°C warmer than TOP during MAM (Figure 3e). A similar pattern is observed in the other seasons—JJA (Figures 3 j–l), SON (Figures 3 p–r), and DJF (Figures 3v–x)—with the smallest TMN bias occurring during DJF relative to the other seasons. This behavior can be explained by the influence of the soil moisture scheme on net downward longwave radiation (RLNS), surface temperature (TS), and ultimately TMN, with differences arising from the contrasting soil moisture dynamics in the TOP and VIC schemes.

Concerning soil moisture initialization, the ESA dataset produces higher soil moisture than CEN, with differences ranging from 7.5 to 22.5 mm and reaching up to 30 mm in the Nile Delta region (Figure 2d–f). Figure S4 presents the radiative analysis for the ESA and CEN simulations. The results indicate that switching between ESA and CEN has minimal impact on incoming shortwave radiation (RSDS; Figures S4a–c), net surface solar radiation (RSNS; Figures S4d–f), or incoming longwave

radiation (RLDS; Figures S4g–i). Net downward longwave radiation (RLNS), however, is influenced by soil moisture initialization, with ESA exceeding CEN by 5–11 W m^{-2} (Figures S4j–l). Thermally, surface temperature (TS) is higher in ESA than CEN by 1–3°C (Figure S5c). No substantial differences are observed between the two simulations for sensible heat flux (SHF) or 2 m relative humidity (RH) (Figures S5d–f and g–i). Notably, TMX remains largely unaffected by the choice of soil moisture dataset. For TMN, ESA generally produces slightly higher values than CEN, with warm and cold biases similar to those observed in the parameterized soil moisture experiments, consistent with the results reported by Anwar (2024).

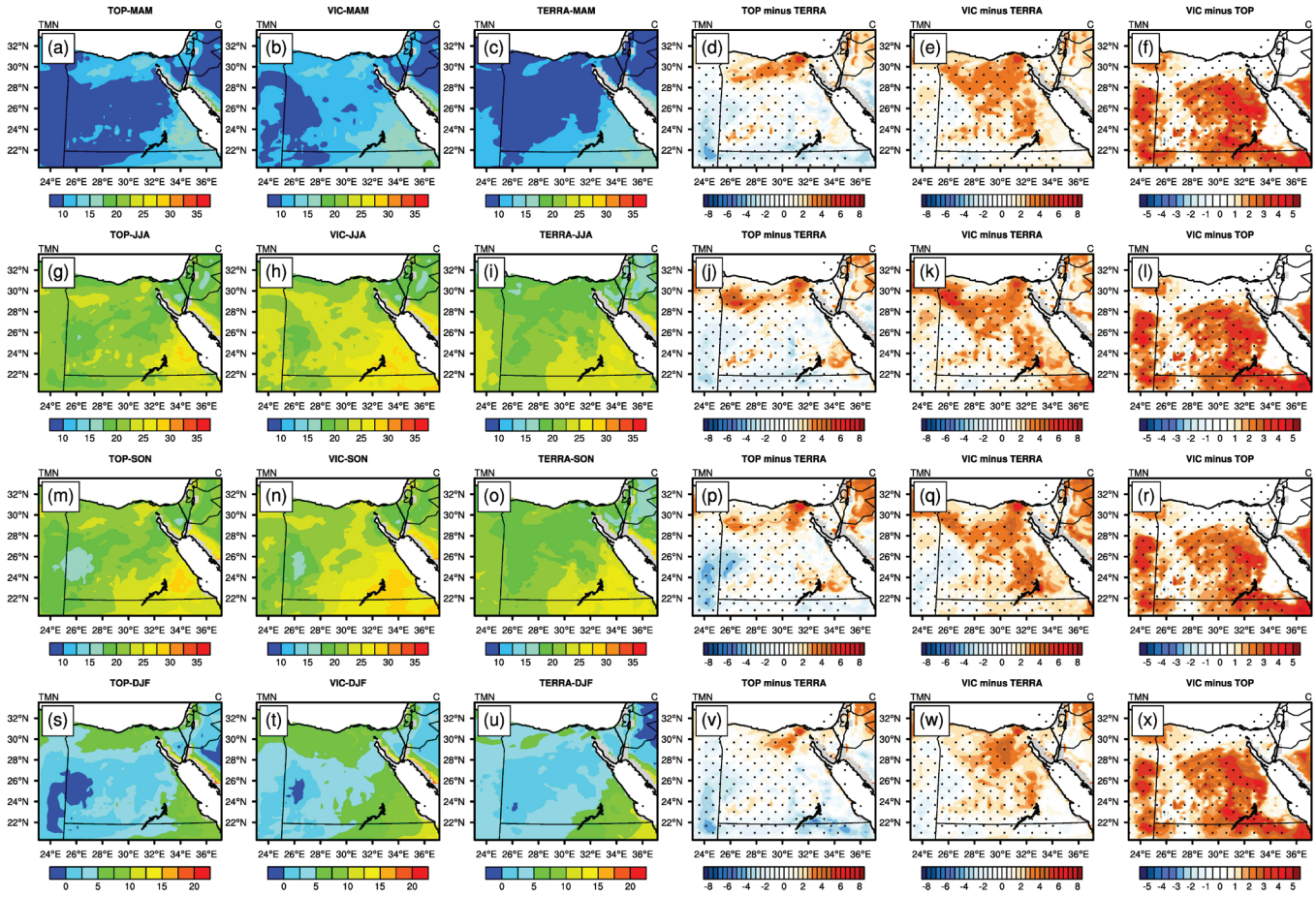

Figure 3: Seasonal climatology of 2-m minimum air temperature (TMN, °C) simulated by the TOP/VIC scheme for spring (MAM), summer (JJA), autumn (SON), and winter (DJF) over the period 1981–2018. Observations from the TERRA reanalysis product were interpolated onto the RegCM4 curvilinear grid for comparison. Statistically significant differences between simulations and reanalysis were assessed using a Student's t-test at α = 0.05. Panels are arranged in chronological order from spring to winter, left to right.

3.2. Influence on the DTR

3.2.1. Seasonal climatology

This section examines the impact of soil moisture initialization and parameterization on the diurnal temperature range (DTR, °C) through their influence on daily maximum (TMX) and minimum (TMN) temperatures. Figure 4 illustrates the seasonal DTR patterns simulated using the TOP and VIC schemes. The results indicate that RegCM4 effectively captures the spatial distribution of DTR relative to the TerraClimateZ (TERRA) dataset across all seasons. Nonetheless, both simulations exhibit a consistent cold bias over Egypt. Overall, the TOP scheme demonstrates better agreement with TERRA than VIC in all seasons. During the MAM season, the TOP simulation exhibited a cold bias of 1–4°C in regions including 22–24°N, 28–30°E, and 28–30°N, 28–30°E (Figure 4d). In contrast, VIC showed a more pronounced cold bias across Egypt, ranging from 2 to 7°C (Figure 4e), making VIC 1–5°C cooler than TOP overall (Figure 4f). A similar pattern was observed in JJA, with TOP maintaining

http://dx.doi.org/10.21622/MACI.2026.03.1.1985

a comparable cold bias to MAM (Figure 4j), while VIC continued to display a 2–7°C cold bias across the country, reaching nearly 8°C in some locations (Figure 4k).

During SON, the spatial pattern shifted: TOP's cold bias was mainly confined to 28–30°E, 28–30°N, whereas a warm bias of 3–4°C appeared along the Red Sea coastline (Figure 4p). VIC, however, exhibited a cold bias ranging from 1.5 to 5.5°C, which was slightly less severe than in JJA (Figure 4q). In DJF, TOP showed a cold bias of 1–4.5°C in certain regions (Figure 4v), while VIC maintained a 2–6°C cold bias, reaching up to 7°C in some areas, and was generally 2–5°C cooler than TOP (Figure 4w–x). For soil moisture initialization, the ESA and CEN simulations (Figure S6) produced TMX and TMN patterns similar to those seen in the TOP and VIC experiments. Based on the results of the diagnostic analyses of TMX, TMN, and DTR (Figures 2 and S1–S5), the CEN-TOP configuration (hereafter RCM) was selected as the most suitable physical setup for accurately simulating DTR. Subsequent analysis evaluated the RCM's ability to reproduce the DTR annual cycle relative to in-situ observations. The added value of the LS bias-correction method was also assessed using mean bias (MB) as a statistical metric.

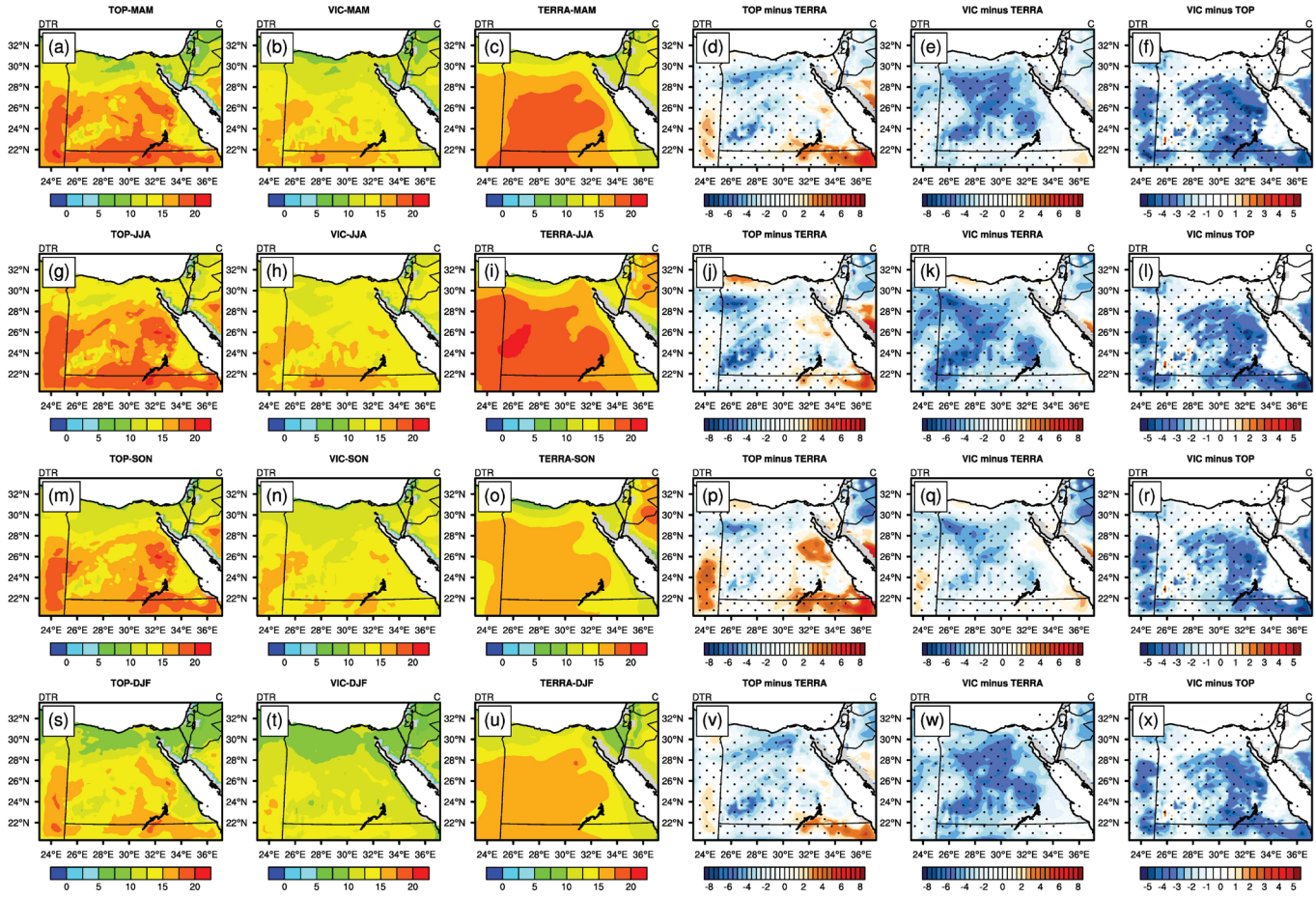

Figure 4: Seasonal climatology of diurnal temperature range (DTR, °C) simulated by the TOP/VIC scheme for spring (MAM), summer (JJA), autumn (SON), and winter (DJF) over the period 1981–2018. TERRA reanalysis data were interpolated onto the RegCM4 curvilinear grid for comparison. Statistically significant differences between simulations and reanalysis were calculated using a Student's t-test at $\alpha = 0.05$. Panels are arranged from spring to winter, left to right.

3.2.2. Annual cycle

The ability of the RCM to Z reproduce the annual cycle of DTR was evaluated at 15 stations using in-situ observations (OBS), both before and after applying the LS bias-correction method. The site-specific biases in TMN and DTR reflect the critical role of soil moisture in modulating surface energy balance and land–atmosphere interactions. Variations in soil moisture influence the partitioning of net radiation into latent and sensible heat fluxes: drier soils limit evapotranspiration,

enhancing sensible heating and increasing daytime temperatures, while wetter soils promote latent heat flux, cooling the surface and affecting nighttime conditions. Soil moisture also impacts ground heat storage and longwave radiation loss, further shaping nighttime temperatures and DTR. Consequently, the magnitude and seasonal timing of TMN and DTR biases at each site can be interpreted in terms of these soil moisture–driven processes, providing a mechanistic basis for understanding the spatial and temporal patterns observed in the model simulations.

- **Alexandria:** Observations show DTR peaks in February, March, November, and December, with minima in July and August, coinciding with the highest relative humidity. Before LS correction, the RCM systematically overestimated DTR (MB = 3.05°C), failing to capture the summer minimum. The overestimation arises from the model underrepresenting soil moisture in summer, limiting latent heat flux and enhancing daytime sensible heating. After LS correction, the RCMnew substantially improved agreement with OBS, reducing MB to 0.01°C, increasing CORR from -0.01 to 0.89, and raising STD from 0.73 to 0.97.

- **Arish:** The observed DTR exhibits two peaks (April & November) and a minimum in August. The uncorrected RCM underestimated DTR in August (MB = -2.1°C), likely due to excessive soil moisture limiting sensible heating during daytime. After LS correction, MB decreased to 0.07°C, CORR improved from 0.21 to 0.62, and STD decreased from 1.55 to 0.95, indicating improved representation of seasonal soil moisture impacts on DTR.

- **Asswan and Assyut:** Observations show DTR peaks in April and September (Asswan) and April and September (Assyut), with minima in July. The uncorrected RCM slightly underestimated DTR (MB = -2.4°C for Asswan, -3.43°C for Assyut). This underestimation is linked to the overestimation of soil moisture during dry periods, which reduces sensible heating. Following LS correction, MB improved to 0.01°C (Asswan) and -0.01°C (Assyut), while CORR and STD remained stable, confirming that soil moisture adjustments effectively corrected the seasonal biases.

- **Cairo:** The RCM slightly overestimated DTR (MB = 0.775°C) before LS correction. After correction, MB decreased to 0.03°C, CORR increased from 0.94 to 0.98, and STD decreased from 1.08 to 0.94. The improvement reflects better representation of surface energy partitioning, with adjusted soil moisture reducing excessive daytime heating and nighttime cooling errors.

- **Dabaa:** The uncorrected RCM underestimated the March peak and overestimated July DTR (MB = 6.38°C). The LS correction reduced MB to 0.22°C and increased CORR from 0.55 to 0.84. The initial bias was driven by the misrepresentation of soil moisture controlling latent and sensible heat fluxes during dry summer months.

- **Dakhla and Farafra:** Both stations showed significant underestimation of DTR in the uncorrected RCM (MB = -5.46°C and -5.7°C), reflecting excessive soil moisture and suppressed daytime heating. LS correction reduced MB to -0.01°C, increased CORR (Dakhla: 0.88 → 0.97), and improved STD (Dakhla: 0.85 → 1; Farafra: 0.66 → 0.95), demonstrating effective correction of soil moisture–related biases.

- **Hurgada:** The uncorrected RCM showed erratic DTR, sometimes inverting the observed annual cycle (MB = -7.83°C, CORR = -0.33). LS correction adjusted soil moisture representation, improving MB to -0.03°C, CORR to 0.72, and STD to 1.01, indicating stronger control of daytime heating and nighttime cooling by soil moisture.

- **Ismailia:** Observed DTR shows two peaks (May, July) and minima (October, December). The RCM slightly underestimated DTR (MB = -2.42°C). LS correction reduced MB to 0.07°C, while STD improved from 1.33 to 0.9, reflecting better soil moisture–driven energy flux partitioning.

- **Luxor:** The uncorrected RCM underestimated DTR (MB = -7.2°C), due to excessive soil moisture limiting sensible heat flux. LS correction improved MB to 0.02°C, CORR from 0.48 to 0.9, and STD from 0.56 to 0.93, capturing both the seasonal cycle and magnitude of DTR.

http://dx.doi.org/10.21622/MACI.2026.03.1.1985

- **Port Said, Ras Sedr, Shallateen:** These stations exhibited varying initial biases (MB = -4.12°C to -8.29°C). LS correction reduced MB to near-zero values (-0.002°C to -0.01°C) and improved CORR and STD across stations.

The adjustments highlight the importance of accurate soil moisture initialization and parameterization in controlling surface fluxes and DTR representation.

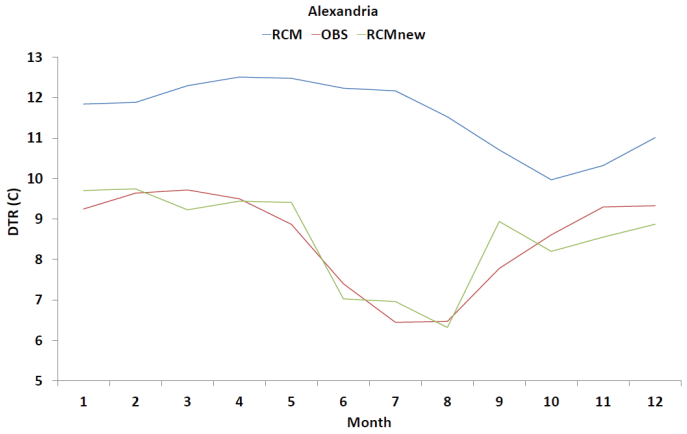

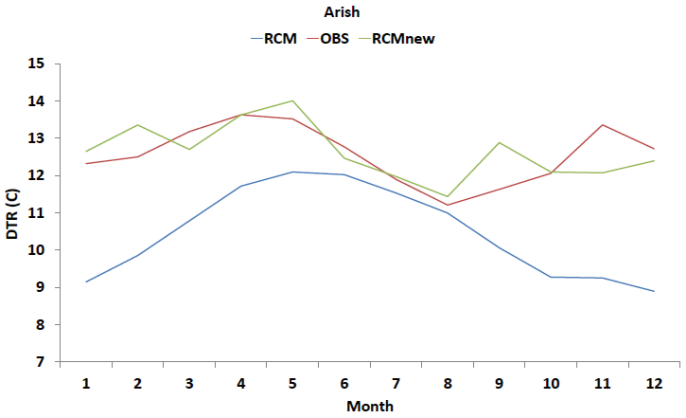

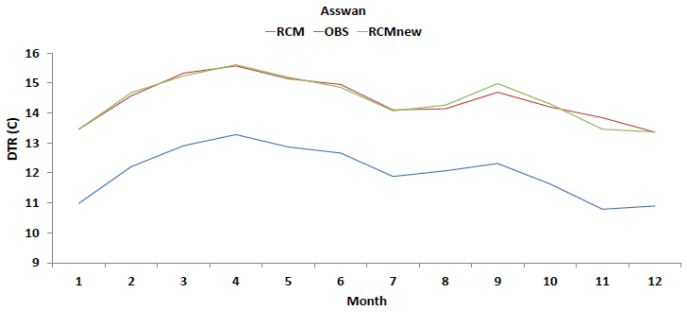

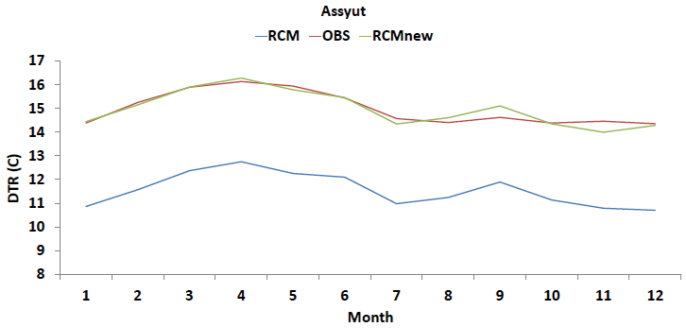

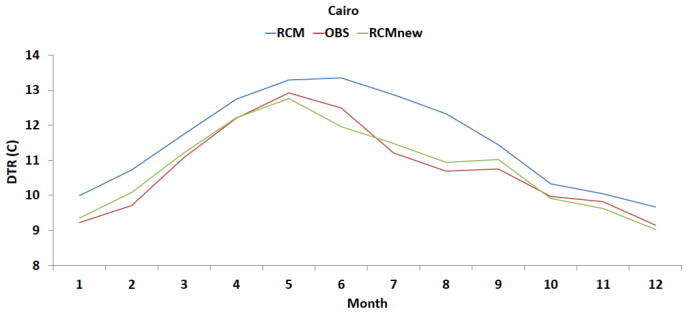

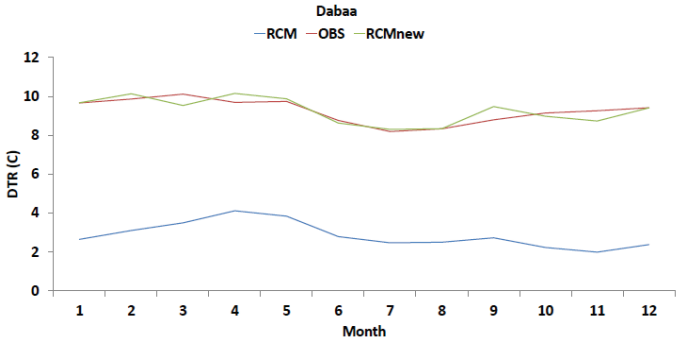

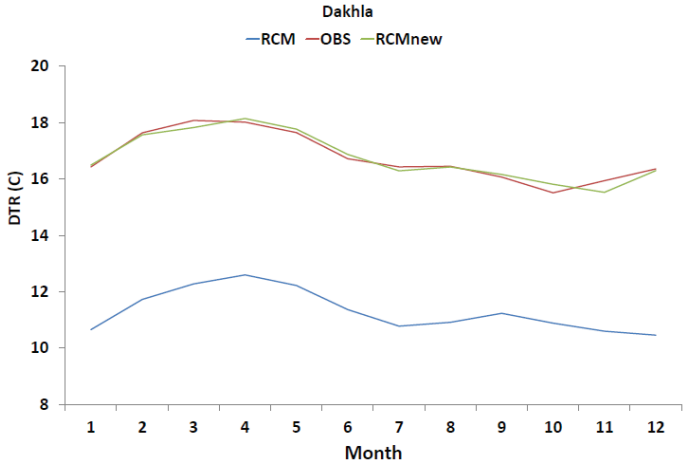

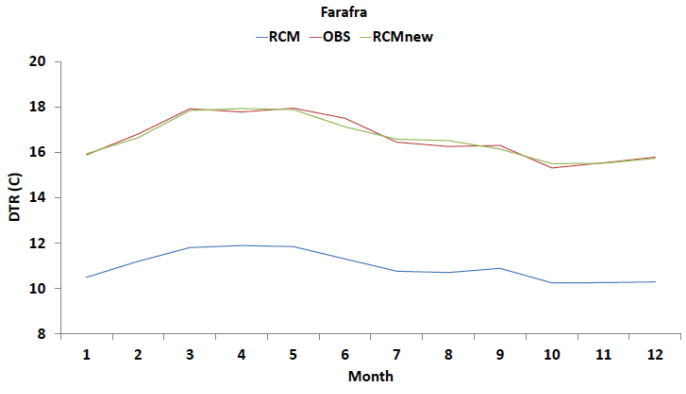

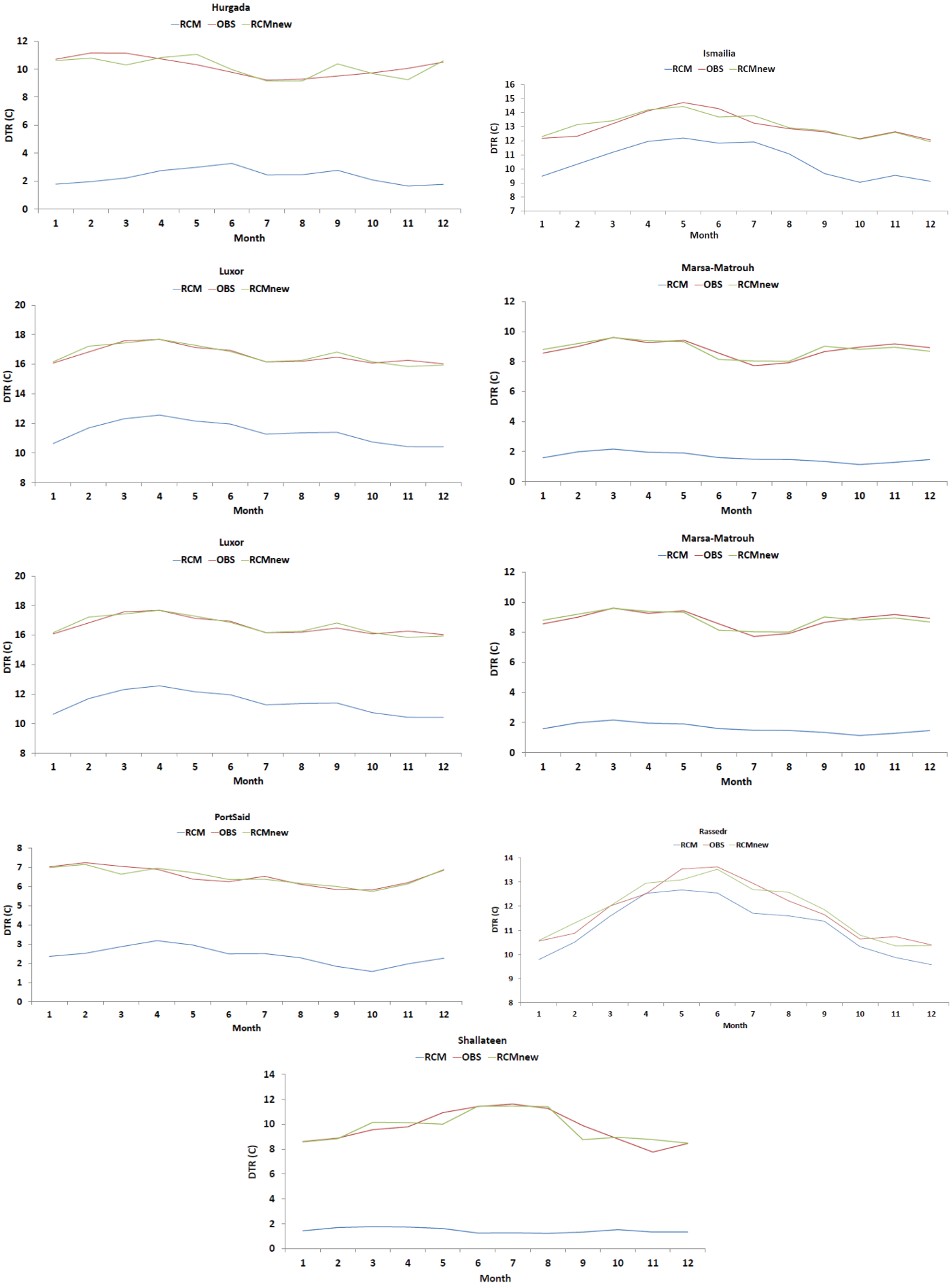

Figure 5: Diurnal temperature range (DTR; °C) annual cycle climatology during the validation period 2001 - 2010. RCM (in blue) refers to the raw data of DTR, RCMnew (in green) is the bias-corrected DTR, and OBS (in red) is the in-situ observation. RCM refers to the CEN-TOP configuration

http://dx.doi.org/10.21622/MACI.2026.03.1.1985

The biases in TMN and DTR discussed above can be directly linked to soil moisture–driven processes, where variations in latent and sensible heat fluxes, as well as land–atmosphere coupling, modulate the diurnal cycle. The quantitative performance of RCM and RCMnew for all 15 sites is summarized in Figure 6 using a Taylor diagram, which provides a consolidated assessment of CORR, STD, and overall agreement with observations. The results consistently demonstrate that the LS bias-correction method substantially improves model performance across all stations, particularly in reducing MB and enhancing correlation with observed DTR. To further facilitate comparison across stations, a summary of key statistical metrics (MB, CORR, and STD) has been added in Table 3.

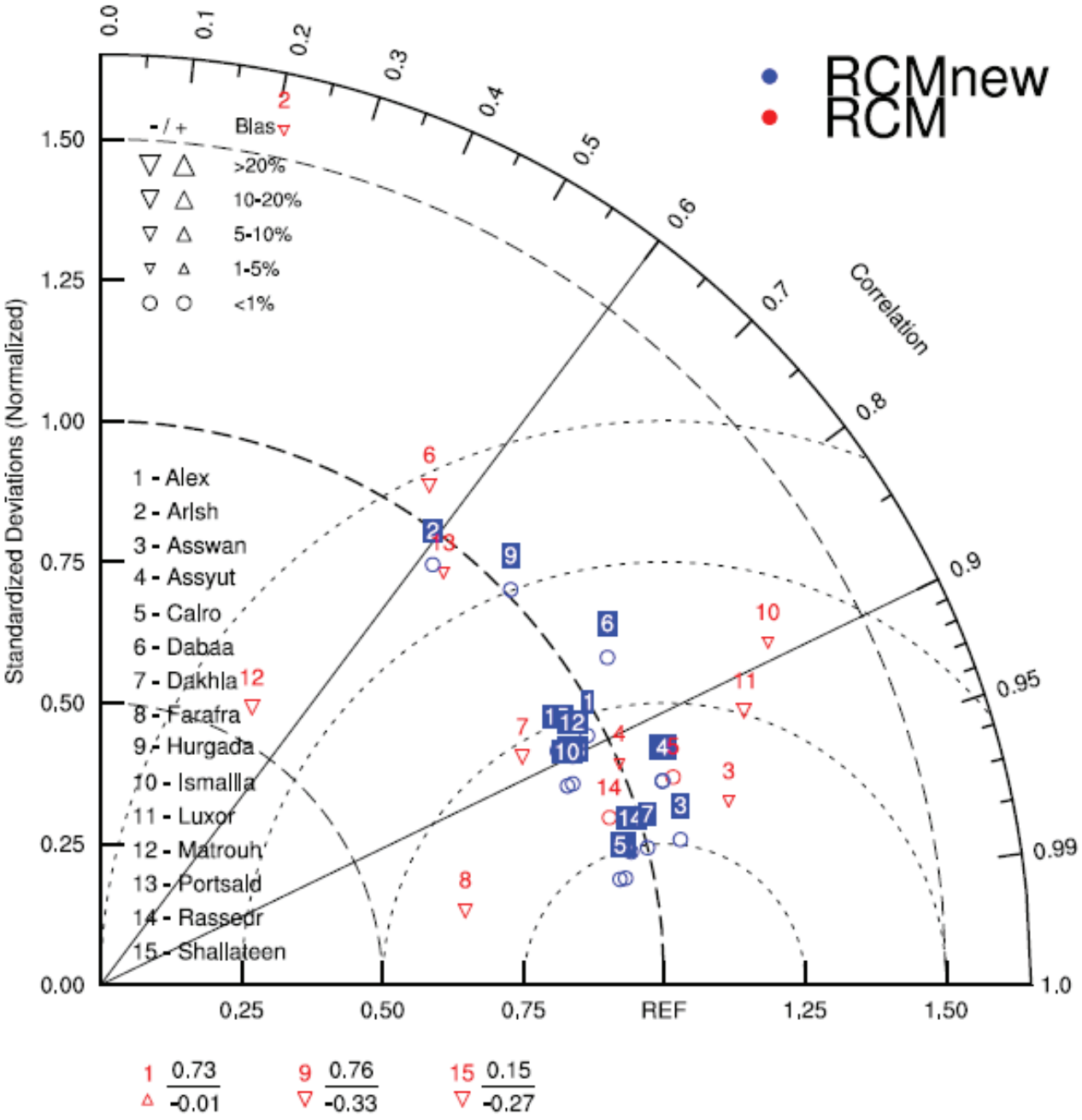

Figure 6: The Taylor diagram explores the performance of the RCM/RCMnew (concerning the OBS) for the 15 locations before and after using the LS method in the period 2001 - 2010

Table 3: Statistical performance of the regional climate model (RCM) and the bias-corrected model (RCMnew) in reproducing the annual cycle of diurnal temperature range (DTR) at 15 stations. Metrics include mean bias (MB; °C), correlation coefficient (CORR), and standard deviation (STD; °C). Missing values (—) indicate cases where the metric was not explicitly reported in the analysis

Station	MB (RCM) °C	MB (RCMnew) °C	CORR (RCM)	CORR (RCMnew)	STD (RCM)	STD (RCMnew)
Alexandria	3.05	0.01	-0.01	0.89	0.73	0.97
Arish	-2.10	0.07	0.21	0.62	1.55	0.95
Aswan	-2.40	0.01	—	—	—	—
Assyut	-3.43	-0.01	—	—	—	—
Cairo	0.78	0.03	0.94	0.98	1.08	0.94
Dabaa	6.38	0.22	0.55	0.84	—	—
Dakhla	-5.46	-0.01	0.88	0.97	0.85	1.00
Farafra	-5.70	-0.01	—	—	0.66	0.95
Hurghada	-7.83	-0.03	-0.33	0.72	0.76	1.01
Ismailia	-2.42	0.07	—	—	1.33	0.90
Luxor	-7.20	0.02	0.48	0.90	0.56	0.93
Port Said	-4.12	-0.01	0.64	0.92	—	—
Ras Sedr	-0.63	0.03	—	—	0.95	0.97
Shallateen	-8.29	-0.002	-0.27	0.89	0.15	0.91

To summarize the results, four 40-year simulations were conducted, representing different combinations of soil moisture datasets and hydrological schemes on the DTR across Egypt. All simulations were downscaled to a 25 km horizontal grid using the ERA-Interim reanalysis at 1.5° (EIN15). The first two simulations focused on soil moisture initialization, while the latter two examined soil moisture parameterization. Model results were evaluated against the high-resolution global TerraClimate (TERRA) dataset at each grid point, and the DTR annual cycle was assessed relative to in-situ observations (OBS).

The main findings can be summarized as follows:

1. TMX was largely unaffected by either soil moisture initialization or hydrological schemes, as neither RSNS nor SHF showed substantial changes.

2. TMN was strongly influenced in both scenarios due to variations in SM and RLNS.

3. Configuring RegCM4 with the TOP scheme and initializing with the CEN reanalysis product effectively reduced TMN and DTR biases relative to TERRA.

4. The ability of the RCM to reproduce the DTR annual cycle relative to OBS varied depending on station location.

5. The LS bias-correction method successfully reduced MB at all stations and generally improved CORR and STD. With LS applied, the RCMnew accurately captured the observed DTR yearly cycle.

The sensitivity of TMN and DTR to soil moisture can be explained by its key role in regulating the surface energy balance and land–atmosphere interactions. Variations in soil moisture influence the partitioning of net radiation into latent and sensible heat fluxes. Under drier conditions, limited soil moisture reduces evapotranspiration, enhancing sensible heating and increasing near-surface air temperatures, particularly during daytime, which contributes to an elevated DTR. In contrast, wetter soils promote latent heat flux and evaporative cooling, reducing daytime temperatures and moderating nighttime conditions. Soil moisture also affects soil heat storage and near-surface atmospheric humidity, influencing RLNS and thereby shaping TMN. Through these processes, the interaction between soil moisture, surface fluxes, and boundary layer dynamics explains the spatial and seasonal variations in DTR biases observed across Egypt.

http://dx.doi.org/10.21622/MACI.2026.03.1.1985

It should be noted that the analysis does not include the most recent years (post-2018), during which accelerated warming has been reported. While the primary findings regarding DTR sensitivity to soil moisture are expected to remain robust, future work could extend the simulations using updated datasets to assess potential impacts of recent climate trends. Although other meteorological drivers—including cloud cover, wind speed, and atmospheric moisture—also influence DTR by affecting daytime heating and nighttime cooling, these factors are implicitly represented in the model simulations. Therefore, the attribution of DTR variability presented here should be interpreted primarily in terms of soil moisture effects within the modeling framework.

4. Conclusion and Future recommendations

The present study employed the Regional Climate Model version 4 (RegCM4) to assess the impact of soil moisture initialization and parameterization on the DTR across Egypt, using high-resolution observational datasets and in situ measurements for evaluation. The key findings are:

1. The CEN-TOP configuration consistently exhibited the lowest bias in simulated DTR relative to the TERRA dataset, highlighting its suitability for regional applications.

2. Application of the linear scaling (LS) bias-correction method effectively reduced mean bias (MB) while improving correlation (CORR) and standard deviation (STD) at all stations, demonstrating its capability to enhance DTR simulations.

These results provide the first systematic assessment of soil moisture–DTR interactions in Egypt and offer a framework for improving regional climate simulations. To further enhance DTR representation, future studies should consider:

1. Incorporating high-resolution geographic data into the static datasets used by RegCM.

2. Employing a convective-permitting setup within the latest RegCM version (RegCM5) to better capture local geographic influences on surface climate.

3. Exploring parameterization uncertainty using alternative regional climate models, such as WRF (Skamarock et al., 2019), ICON (Hohenegger et al., 2023), and REMO (Pietikäinen et al., 2018), and comparing LS with other bias-correction methods, including power transformation (PT), distribution mapping (DM), and quantile mapping (QM), to assess their relative strengths and limitations.

Overall, the study demonstrates that accurate DTR simulations in Egypt require careful consideration of soil moisture initialization and parameterization, combined with appropriate bias-correction techniques, providing a valuable reference for future climate modeling and adaptation planning.

Author Contributions: All aspects of the study were performed by Anwar SA, including conceptualization, methodology, software, validation, formal analysis, investigation, resources, data curation, writing—original draft preparation, writing—review and editing, visualization, supervision, and project administration. All authors have read and approved the published version of the manuscript.

Funding: No funding was received for this study.

Institutional Review Board Statement: Not applicable.

Data Availability Statement: Not applicable.

Informed Consent Statement: Not applicable.

Acknowledgments: Egyptian Meteorological Authority (EMA) is acknowledged for providing the computational power to conduct the RegCM4 simulations and station observations to evaluate the RegCM4 performance in different locations.

Conflicts of Interest: There is no conflict of interest.

References:

Adekanmbi, A. A., & Sizmur, T. (2022). Importance of Diurnal Temperature Range (DTR) for predicting the temperature sensitivity of soil respiration. *Frontiers in Soil Science*, *2*. https://doi.org/10.3389/fsoil.2022.969077

Anwar, S. A. Simulating Daily Soil Temperature in Egypt Using a High-Resolution Regional Climate Model: Sensitivity to Soil Moisture and Temperature Initial Conditions. *Eng. Proc. 2023*, 56, 106. https://doi.org/10.3390/ASEC2023-15368

Anwar, S. A. (2024). On the Sensitivity of the Potential Evapotranspiration of Egypt to Different Initial Conditions of the Soil Moisture Using a High-resolution Regional Climate Model. *Journal of Biomedical Research & Environmental Sciences*, *5*(5), 501–514. https://doi.org/10.37871/jbres1920

Anwar, S. A., A.S. Zakey, S.M. Robaa, & Abdel, M. (2018). The influence of two land-surface hydrology schemes on the regional climate of Africa using the RegCM4 model. *Theoretical and Applied Climatology*, *136*(3-4), 1535–1548. https://doi.org/10.1007/s00704-018-2556-8

Anwar, S. A., & Mostafa, S. M. Assessment of the Sensitivity of Daily Maximum and Minimum Air Temperatures of Egypt to Soil Moisture Status and Land Surface Parameterization Using RegCM4. *Eng. Proc. 2023*, 56, 115. https://doi.org/10.3390/ASEC2023-15353

Anwar, S. A., & Olusegun, C. F. (2024). Simulating the Potential Evapotranspiration of Egypt Using the RegCM4: Sensitivity to the Land Surface and Boundary Layer Parameterizations. *Hydrology*, *11*(8), 121. https://doi.org/10.3390/hydrology11080121

Braganza, K., Karoly, D. J., & Arblaster, J. M. (2004). Diurnal temperature range as an index of global climate change during the twentieth century. *Geophysical Research Letters*, *31*(13), n/a-n/a. https://doi.org/10.1029/2004gl019998

Bravo Dias, J., Soares, P. M. M., & Carrilho da Graça, G. (2020). The shape of days to come: Effects of climate change on low energy buildings. *Building and Environment*, *181*, 107125. https://doi.org/10.1016/j.buildenv.2020.107125

Dai, A., Trenberth, K. E., & Karl, T. R. (1999). Effects of Clouds, Soil Moisture, Precipitation, and Water Vapor on Diurnal Temperature Range. *Journal of Climate*, *12*(8), 2451–2473. https://doi.org/10.1175/1520-0442(1999)012%3C2451:eocsmp%3E2.0.co;2

Davis, R. E., Hondula, D. M., & Sharif, H. (2019). Examining the diurnal temperature range enigma: why is human health related to the daily change in temperature? *International Journal of Biometeorology*, *64*(3), 397–407. https://doi.org/10.1007/s00484-019-01825-8

Dee, D. P., Uppala, S. M., Simmons, A. J., Berrisford, P., Poli, P., Kobayashi, S., ... Haimberger, L. (2011). The ERA-Interim reanalysis: configuration and performance of the data assimilation system. *Quarterly Journal of the Royal Meteorological Society*, *137*(656), 553–597. https://doi.org/10.1002/qj.828

Dorigo, W., Wagner, W., Albergel, C., Albrecht, F., Balsamo, G., Brocca, L., ... Mistelbauer, T. (2017). ESA CCI Soil Moisture for improved Earth system understanding: State-of-the art and future directions. *Remote Sensing of Environment*, *203*, 185–215. https://doi.org/10.1016/j.rse.2017.07.001

El Kenawy, A., López-Moreno, J., M.Vicente-Serrano, S., & Morsi, F. (2010). Climatological modeling of monthly air temperature and precipitation in Egypt through GIS techniques. *Climate Research*, *42*(2), 161–176. https://doi.org/10.3354/cr00871

Emanuel, K. A., & Živković-Rothman, M. (1999). Development and Evaluation of a Convection Scheme for Use in Climate Models. *Journal of the Atmospheric Sciences*, *56*(11), 1766–1782. https://doi.org/10.1175/1520-0469(1999)056%3C1766:DAEOAC%3E2.0.CO;2

http://dx.doi.org/10.21622/MACI.2026.03.1.1985

Giorgi, F., Coppola, E., Solmon, F., Mariotti, L., Sylla, M., Bi, X., ... Sloan, L. (2012). RegCM4: model description and preliminary tests over multiple CORDEX domains. *Climate Research*, *52*, 7–29. https://doi.org/10.3354/cr01018

Grell, G. A. ,. (1994). Description of the Penn State/NCAR Mesoscale Model Version 4 (MM4). *NCAR Tech. Note TN-282+STR, NCAR, Boulder, CO*.

Grell, G. A., Dudhia, J., & Stauffer, D. (1994). A description of the fifth-generation Penn State/NCAR Mesoscale Model (MM5). *NCAR Tech. Note TN-282+STR, NCAR, Boulder, CO*. https://doi.org/10.5065/D60Z716B

Grenier, H., & Bretherton, C. S. (2001). A Moist PBL Parameterization for Large-Scale Models and Its Application to Subtropical Cloud-Topped Marine Boundary Layers. *Monthly Weather Review* , *129*(3), 357–377.

Gruber, A., Scanlon, T., van der Schalie, R., Wagner, W., & Dorigo, W. (2019). Evolution of the ESA CCI Soil Moisture climate data records and their underlying merging methodology. *Earth System Science Data*, *11*(2), 717–739. https://doi.org/10.5194/essd-11-717-2019

Güttler, I., Branković, Č., O'Brien, T. A., Coppola, E., Grisogono, B., & Giorgi, F. (2013). Sensitivity of the regional climate model RegCM4.2 to planetary boundary layer parameterisation. *Climate Dynamics*, *43*(7-8), 1753–1772. https://doi.org/10.1007/s00382-013-2003-6

Hamed, M. M., Nashwan, M. S., & Shahid, S. (2021). Intercomparison of historical simulation and future projections of rainfall and temperature by CMIP5 and CMIP6 GCMs over Egypt. *International Journal of Climatology*. https://doi.org/10.1002/joc.7468

Hamed, M. M., Nashwan, M. S., Shiru, M. S., & Shahid, S. (2022). Comparison between CMIP5 and CMIP6 Models over MENA Region Using Historical Simulations and Future Projections. *Sustainability*, *14*(16), 10375. https://doi.org/10.3390/su141610375

Harris, I., Osborn, T. J., Jones, P., & Lister, D. (2020). Version 4 of the CRU TS monthly high-resolution gridded multivariate climate dataset. *Scientific Data*, *7*(1). https://doi.org/10.1038/s41597-020-0453-3

Hohenegger, C., Korn, P., Leonidas Linardakis, Redler, R., Schnur, R., Panagiotis Adamidis, ... Giorgetta, M. (2023). ICON-Sapphire: simulating the components of the Earth system and their interactions at kilometer and subkilometer scales. *Geoscientific Model Development*, *16*(2), 779–811. https://doi.org/10.5194/gmd-16-779-2023

Huang, Y., Jiang, N., Shen, M., & Guo, L. (2020). Effect of preseason diurnal temperature range on the start of vegetation growing season in the Northern Hemisphere. *Ecological Indicators*, *112*, 106161–106161. https://doi.org/10.1016/j.ecolind.2020.106161

Intergovernmental Panel on Climate Change (IPCC). (2021). Climate change 2021: The physical science basis. Contribution of Working Group I to the Sixth Assessment Report of the Intergovernmental Panel on Climate Change. Retrieved from IPCC website: https://www.ipcc.ch/report/ar6/wg1/

Jeong, S.-J., Ho, C.-H., Park, T.-W., Kim, J., & Levis, S. (2010). Impact of vegetation feedback on the temperature and its diurnal range over the Northern Hemisphere during summer in a 2 × CO2 climate. *Climate Dynamics*, *37*(3-4), 821–833. https://doi.org/10.1007/s00382-010-0827-x

Kiehl, J. T., Hack, J. J., Bonan, G. B., Boville, B. A., & Rasch, P. J. (1996, January 1). Description of the NCAR community climate model (CCM3). NCAR Tech. Note NCAR/TN-420+STR.

Kobayashi, C., & Iwasaki, T. (2016). Brewer-Dobson circulation diagnosed from JRA-55. *Journal of Geophysical Research: Atmospheres*, *121*(4), 1493–1510. https://doi.org/10.1002/2015jd023476

Liang, X. (2003). A new parameterization for surface and groundwater interactions and its impact on water budgets with the variable infiltration capacity (VIC) land surface model. *Journal of Geophysical Research*, *108*(D16). https://doi.org/10.1029/2002jd003090

Liang, X., Lettenmaier, D. P., & Wood, E. F. (1996). One-dimensional statistical dynamic representation of subgrid spatial variability of precipitation in the two-layer variable infiltration capacity model. *Journal of Geophysical Research: Atmospheres*, *101*(D16), 21403–21422. https://doi.org/10.1029/96jd01448

Liang, X., Lettenmaier, D. P., Wood, E. F., & Burges, S. J. (1994). A simple hydrologically based model of land surface water and energy fluxes for general circulation models. *Journal of Geophysical Research*, *99*(D7), 14415. https://doi.org/10.1029/94jd00483

Liang, X., Wood, E. F., & Lettenmaier, D. P. (1996). Surface soil moisture parameterization of the VIC-2L model: Evaluation and modification. *Global and Planetary Change*, *13*(1-4), 195–206. https://doi.org/10.1016/0921-8181(95)00046-1

Mlawer, E. J., Taubman, S. J., Brown, P. D., Iacono, M. J., & Clough, S. A. (1997). Radiative transfer for inhomogeneous atmospheres: RRTM, a validated correlated-k model for the longwave. *Journal of Geophysical Research: Atmospheres*, *102*(D14), 16663–16682. https://doi.org/10.1029/97jd00237

Nashwan, M. S., Shahid, S., & Chung, E.-S. (2020). High-Resolution Climate Projections for a Densely Populated Mediterranean Region. *Sustainability*, *12*(9), 3684. https://doi.org/10.3390/su12093684

Niu, G.-Y., Yang, Z.-L., Dickinson, R. E., & Gulden, L. E. (2005). A simple TOPMODEL-based runoff parameterization (SIMTOP) for use in global climate models. *Journal of Geophysical Research*, *110*(D21). https://doi.org/10.1029/2005jd006111

Oleson, K. W., Niu, G.-Y. ., Yang, Z.-L. ., Lawrence, D. M., Thornton, P. E., Lawrence, P. J., … Qian, T. (2008). Improvements to the Community Land Model and their impact on the hydrological cycle. *Journal of Geophysical Research: Biogeosciences*, *113*(G1), n/a-n/a. https://doi.org/10.1029/2007jg000563

Oleson, K., Lawrence, M., Bonan, B., Drewniak, B., Huang, M., Koven, D., … Lipscomb, W. (2013). Technical description of version 4.5 of the Community Land Model (CLM). *N2t.net*. https://doi.org/10.5065/D6RR1W7M

Ongoma, V., Rahman, M. A., Ayugi, B., Nisha, F., Galvin, S., Shilenje, Z. W., & Ogwang, B. A. (2020). Variability of diurnal temperature range over Pacific Island countries, a case study of Fiji. *Meteorology and Atmospheric Physics*, *133*(1), 85–95. https://doi.org/10.1007/s00703-020-00743-4

Pal, J. S., Giorgi, F., Bi, X., Elguindi, N., Solmon, F., Gao, X., … Steiner, A. L. (2007). Regional Climate Modeling for the Developing World: The ICTP RegCM3 and RegCNET. *Bulletin of the American Meteorological Society*, *88*(9), 1395–1410. https://doi.org/10.1175/BAMS-88-9-1395

Panwar, A., Renner, M., & Kleidon, A. (2020). Imprints of evaporative conditions and vegetation type in diurnal temperature variations. *Hydrology and Earth System Sciences*, *24*(10), 4923–4942. https://doi.org/10.5194/hess-24-4923-2020

Pietikäinen, J.-P., Markkanen, T., Sieck, K., Jacob, D., Korhonen, J., Räisänen, P., … Kaurola, J. (2018). The regional climate model REMO (v2015) coupled with the 1-D freshwater lake model FLake (v1): Fenno-Scandinavian climate and lakes. *Geoscientific Model Development*, *11*(4), 1321–1342. https://doi.org/10.5194/gmd-11-1321-2018

Ren, G., & Zhou, Y. (2014). Urbanization Effect on Trends of Extreme Temperature Indices of National Stations over Mainland China, 1961–2008. *Journal of Climate*, *27*(6), 2340–2360. https://doi.org/10.1175/jcli-d-13-00393.1

http://dx.doi.org/10.21622/MACI.2026.03.1.1985

Ritchie, H., Rosado, P., & Roser, M. (2023). CO_2 and Greenhouse Gas Emissions. *Our World in Data*. Our World in Data. Retrieved from https://ourworldindata.org/co2-and-greenhouse-gas-emissions

Schultz, N. M., Lawrence, P. J., & Lee, X. (2017). Global satellite data highlights the diurnal asymmetry of the surface temperature response to deforestation. *Journal of Geophysical Research: Biogeosciences*, *122*(4), 903–917. https://doi.org/10.1002/2016jg003653

Shen, X., Liu, B., & Lu, X. (2017). Effects of land use/land cover on diurnal temperature range in the temperate grassland region of China. *Science of the Total Environment*, *575*, 1211–1218. https://doi.org/10.1016/j.scitotenv.2016.09.187

Skamarock, W. C., Klemp, J. B., Dudhia, J., Gill, D. O., Liu, Z., Berner, J., ... Huang, X.-Y. (2019). Description of the Advanced Research WRF Version 4. *NCAR Technical Notes NCAR/TN-556+STR*.

Slivinski, L. C., Compo, G. P., Whitaker, J. S., Sardeshmukh, P. D., Giese, B. S., McColl, C., ... Domínguez-Castro, F. (2019). Towards a more reliable historical reanalysis: Improvements for version 3 of the Twentieth Century Reanalysis system. *Quarterly Journal of the Royal Meteorological Society*, *145*(724), 2876–2908. https://doi.org/10.1002/qj.3598

Steiner, A. L., Pal, J. S., Rauscher, S. A., Bell, J. L., Diffenbaugh, N. S., Boone, A., ... Giorgi, F. (2009). Land surface coupling in regional climate simulations of the West African monsoon. *Climate Dynamics*, *33*(6), 869–892. https://doi.org/10.1007/s00382-009-0543-6

Stone, D., & Weaver, A. (2003). Factors contributing to diurnal temperature range trends in twentieth and twenty-first century simulations of the CCCma coupled model. *Climate Dynamics*, *20*(5), 435–445. https://doi.org/10.1007/s00382-002-0288-y

Taylor, K. E. (2001). Summarizing multiple aspects of model performance in a single diagram. *Journal of Geophysical Research: Atmospheres*, *106*(D7), 7183–7192. https://doi.org/10.1029/2000jd900719

Wang, F., Zhang, C., Peng, Y., & Zhou, H. (2013). Diurnal temperature range variation and its causes in a semiarid region from 1957 to 2006. *International Journal of Climatology*, *34*(2), 343–354. https://doi.org/10.1002/joc.3690